Available online at www.sciencedirect.com
SCIENCE DIRECT®
Wave Motion 42 (2005) 143–154
WAVE MOTION
www.elsevier.com/locate/wavemoti

Long waves propagating over a circular bowl pit

Kyung-Duck Suh [a,*], Tae-Hwa Jung [a], Merrick C. Haller [b]

[a] *School of Civil, Urban, and Geosystem Engineering, Seoul National University, San 56-1, Shinlim-Dong, Gwanak-Gu, Seoul 151-742, Republic of Korea*
[b] *Department of Civil, Construction, and Environmental Engineering, Oregon State University, 202 Apperson Hall, Corvallis, OR 97331-2302, USA*

Received 15 July 2004; received in revised form 28 December 2004; accepted 10 January 2005
Available online 2 February 2005

Abstract

An analytic solution to the mild slope wave equation is derived for long waves propagating over a circular, bowl-shaped pit located in an otherwise constant depth region. The analytic solution is shown to reduce to a previously derived analytic solution for the case of a bowl-shaped enclosed basin and to agree well with a numerical solution of the hyperbolic mild-slope equations. The effects of the pit dimensions on wave scattering are discussed based on the analytic solution. This analytic solution can also be applied to pits of different general shapes. Finally, wave attenuation in the region over the pit is discussed.

Keywords: Long waves; Analytic solution; Mild slope wave equation; Bowl pit

1. Introduction

As surface gravity waves propagate from the deep ocean to the coast, they are transformed continuously by shoaling, refraction, diffraction, and reflection until they break and dissipate. Numerous numerical models have been developed that include the above phenomena and predict the transformation of waves. However, since numerical solution techniques inherently involve approximations, it is necessary to test these models against both analytic solutions and laboratory and field data from representative cases. In theory, the most rigorous test cases would involve comparisons with laboratory and field data, because they are the physical systems of interest. However, such comparisons can be problematic, since it is difficult to measure all the necessary boundary and forcing conditions, especially in field experiments. Comprehensive measurements are somewhat easier to obtain (and repeat) in a

* Corresponding author. Tel. : +82 2 880 8760; fax: +82 2 887 0349.
E-mail addresses: kdsuh@snu.ac.kr (K.-D. Suh), togye176@snu.ac.kr (T.-H. Jung), hallerm@engr.orst.edu (M.C. Haller).

0165-2125/$ – see front matter © 2005 Elsevier B.V. All rights reserved.
doi:10.1016/j.wavemoti.2005.01.002

laboratory setting, yet difficulties arise when trying to reproduce the laboratory wave generating and absorbing systems in numerical models. Also, experimental data always contain a certain amount of measurement errors.

Analytic solutions are another avenue for testing numerical models. While comparisons with physical data are a good test of whether the physics of the model are complete, comparisons with analytic solutions are a direct test of the numerical model scheme under idealized conditions. These comparisons are also useful for model development, and an advantage of analytic solutions is that they are generally developed at reduced cost, time, and labor in comparison to experiments. In addition, it is often simpler to use the analytic solution as a basis for evaluating the influence of specific forcing or boundary conditions on the problem. Nonetheless, most wave transformation problems are complex, and analytic solutions are available for only special situations.

A frequently considered problem in analytic studies of long wave transformation is the long wave motion around a circular island mounted on an axi-symmetric shoal. Homma [4], Vastano and Reid [13], Jonsson et al. [5], and Zhu and Zhang [16] studied long waves around a circular island mounted on a parabolic or conical shoal. Also, Zhang and Zhu [15] and Fujima et al. [2] presented the solution around a conical island or over a parabolic shoal. Recently, Yu and Zhang [14] presented a more general solution by describing the radial topography of the shoal by a power of the radial distance.

In contrast, the present analytic study considers long waves propagating over a circular, bowl-shaped pit located in an otherwise constant depth region. In addition to providing an analytic solution for use in verifying numerical wave models, this new solution can be used to further study wave transformation over a bowl pit. Such a process is of practical interest, for example, in the analysis of shoreline response in the lee of bathymetric anomalies created by the dredging of nearshore sands (see Michalsen et al. [10] and references therein). In the following section, we derive an analytic solution to the mild slope wave equation for long waves propagating over a circular bowl pit. The analytic solution is then compared with a previously derived analytic solution for a related bottom geometry, and a numerical solution based on the hyperbolic form of the mild slope equation. We also discuss the effects of the pit dimensions on the wave scattering using our analytic solution. Finally, wave attenuation in the region over the pit is discussed, and then we summarize the main conclusions.

2. Analytic solution

Consider an axi-symmetric bowl-shaped pit situated in an otherwise constant depth region as shown in Fig. 1, where the origin of the horizontal coordinate system is taken to be the center of the pit, r is the radial distance from the origin, and θ is the angle measured counterclockwise from the positive x-axis. The incident wave is assumed to be a long-crested wave propagating in the positive x direction. The water depths at the origin and in the constant

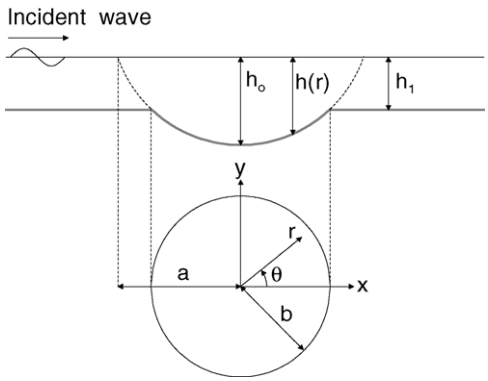

Fig. 1. Definition sketch of a circular bowl pit located in an otherwise constant depth region.

depth region are denoted by h_0 and h_1, respectively. The water depth in the pit is taken as the shape of a paraboloid and decreases gradually from the center to the edge, according to the law, $h = h_0(1 - r^2/a^2)$, where a is the radial distance from the pit center to the imaginary edge of the pit extended to the water surface. Denoting the radial distance to the actual edge of the pit as b, the water depth is given by

$$h = \begin{cases} h_0\left(1 - \dfrac{r^2}{a^2}\right), & r < b \\ h_1 = h_0\left(1 - \dfrac{b^2}{a^2}\right), & r \geq b \end{cases} \tag{1}$$

The mild slope wave equation is given by

$$\nabla \cdot (CC_g \nabla\eta) + k^2 CC_g \eta = 0 \tag{2}$$

where η is the complex water surface elevation, C the phase speed, C_g the group velocity, k the wave number, and ∇ is the horizontal gradient operator. For long (shallow water) waves, $C \cong C_g \cong \sqrt{gh}$ and $\sigma^2 \cong gk^2 h$, where g is the gravitational acceleration, h the water depth, and σ is the angular frequency of the waves. Thus, for long waves, Eq. (2) becomes

$$h\nabla^2\eta + \nabla h \cdot \nabla\eta + \frac{\sigma^2}{g}\eta = 0 \tag{3}$$

In the pit area where $h = h(r)$, this equation can be expressed in polar coordinates as

$$h\left(\frac{\partial^2\eta}{\partial r^2} + \frac{1}{r}\frac{\partial\eta}{\partial r} + \frac{1}{r^2}\frac{\partial^2\eta}{\partial\theta^2}\right) + \frac{\mathrm{d}h}{\mathrm{d}r}\frac{\partial\eta}{\partial r} + \frac{\sigma^2}{g}\eta = 0 \tag{4}$$

Using the method of separation of variables, i.e., by assuming η as a product form:

$$\eta(r, \theta) = R(r)\Theta(\theta) \tag{5}$$

we obtain an eigenvalue problem for Θ, which leads to

$$\Theta_n(\theta) = C_{1n}\cos n\theta + C_{2n}\sin n\theta \quad (n = 0, 1, 2, \ldots) \tag{6}$$

where C_{1n} and C_{2n} are arbitrary constants. The function $R(r)$ corresponding to each eigenvalue n can then be shown to satisfy the following ordinary differential equation:

$$(a^2 - r^2)r^2\frac{\mathrm{d}^2 R_n}{\mathrm{d}r^2} + (a^2 r - 3r^3)\frac{\mathrm{d}R_n}{\mathrm{d}r} + (\nu^2 r^2 - n^2 a^2 + n^2 r^2)R_n = 0 \tag{7}$$

where ν is given by

$$\nu = \frac{\sigma a}{\sqrt{gh_0}} \tag{8}$$

The integral of Eq. (7) takes the form of a Frobenius series [3]:

$$R_n(r) = \sum_{m=0}^{\infty} \alpha_{m,n} r^{m+c} \tag{9}$$

with $\alpha_{0,n}$ being unity and c is a constant to be determined by the indicial equation. According to the Frobenius solution, the series converges for $r < a$. Thus, the solution always converges in the pit region of $r < b$.

The indicial equation, $c^2 - n^2 = 0$, gives two different integers for c:

$$c = \pm n \tag{10}$$

which, in turn, give two linearly independent solutions:

$$R_{n,1} = \sum_{m=0}^{\infty} \alpha_{m,n} r^{m+n} \tag{11}$$

$$R_{n,2} = R_{n,1} \ln r + \sum_{m=0}^{\infty} \beta_{m,n} r^{m-n} \tag{12}$$

Imposing the condition that water surface elevation must be finite at the origin, $R_{n,2}$ can be omitted.

Comparing Eqs. (9) and (11), we obtain

$$c = n \tag{13}$$

Substituting Eq. (9) with $c = n$ into Eq. (7) and collecting the terms of the same order of r, we obtain

$$\alpha_{1,n} = 0 \tag{14}$$

$$\alpha_{m+2,n} = \frac{(m+n)(m+n+2) - \nu^2 - n^2}{a^2(m+2)(m+2n+2)} \alpha_{m,n} \quad (m = 0, 1, 2, \ldots) \tag{15}$$

Finally, for long waves over a bowl pit, the water surface elevation is given by

$$\eta = \sum_{n=0}^{\infty} A_n R_n (C_{1n} \cos n\theta + C_{2n} \sin n\theta) \tag{16}$$

where A_n is an arbitrary constant.

The long-crested incident wave propagating in the positive x direction can be represented by

$$\eta_0 = a_i \mathrm{e}^{ikx} \tag{17}$$

where a_i is the incident wave amplitude and $i = \sqrt{-1}$. It is known that η_0 can be expanded into

$$\eta_0 = a_i \sum_{n=0}^{\infty} i^n \varepsilon_n J_n(kr) \cos n\theta \tag{18}$$

where J_n is the Bessel function of the first kind of order n, and ε_n is the Jacobi symbol defined by

$$\varepsilon_n = \begin{cases} 1, & n = 0 \\ 2, & n \geq 1 \end{cases} \tag{19}$$

In order to obtain the full solution, we apply the method of matched eigen-expansions. Accordingly, we divide the fluid domain into two regions in the horizontal plane: the finite region with variable depth ($r < b$), and the semi-infinite far region with constant depth ($r \geq b$). In the far region, the general solution of the complex surface elevation satisfies the Sommerfeld radiation condition at infinity as well as the symmetry condition about the x-axis and can be written as

$$\eta_1 = \eta_0 + \sum_{n=0}^{\infty} D_n H_n^{(1)}(kr) \cos n\theta, \quad r \geq b \tag{20}$$

where D_n is a set of complex constants to be determined, and $H_n^{(1)}$ is the Hankel function of the first kind of order n.

In the finite region with varying depth, the water surface elevation can be written as follows:

$$\eta_2 = \sum_{n=0}^{\infty} B_n R_n \cos n\theta \tag{21}$$

where $B_n = A_n C_{1n}$ is again a set of complex constants to be determined. The terms associated with $\sin n\theta$ have been dropped based on the symmetry condition.

At $r = b$, the dynamic and kinematic matching conditions require

$$\eta_1 = \eta_2 \quad \text{at } r = b \tag{22}$$

$$\frac{\partial \eta_1}{\partial r} = \frac{\partial \eta_2}{\partial r} \quad \text{at } r = b \tag{23}$$

Substituting Eqs. (20) and (21) into Eqs. (22) and (23) while noting that $\{\cos n\theta\}$ form an orthogonal set, we have

$$B_n R_n(b) = a_i i^n \varepsilon_n J_n(kb) + D_n H_n^{(1)}(kb) \tag{24}$$

$$B_n R_n'(b) = a_i k i^n \varepsilon_n J_n'(kb) + k D_n H_n^{(1)\prime}(kb) \tag{25}$$

where the prime denotes derivatives. Solving for B_n and D_n, we find

$$B_n = a_i k i^n \varepsilon_n \frac{J_n(kb) H_n^{(1)\prime}(kb) - J_n'(kb) H_n^{(1)}(kb)}{k R_n(b) H_n^{(1)\prime}(kb) - R_n'(b) H_n^{(1)}(kb)} \tag{26}$$

$$D_n = a_i i^n \varepsilon_n \frac{k J_n'(kb) R_n(b) - J_n(kb) R_n'(b)}{H_n^{(1)}(kb) R_n'(b) - k H_n^{(1)\prime}(kb) R_n(b)} \tag{27}$$

Substituting these coefficients back into Eqs. (20) and (21), we can compute the water surface elevation for the whole domain.

3. Results and discussions

3.1. Comparison with previously derived analytic solution

In the case that the bowl pit extends to the water surface, or $a = b$ in Fig. 1, Lamb [6] derived the solution for $R(r)$ as

$$R(r) = \sum_{n=0}^{\infty} R_n(r) = \sum_{n=0}^{\infty} \sum_{m=n}^{\infty} A_{m,n} \left(\frac{r}{a}\right)^m \tag{28}$$

with the relation between consecutive coefficients:

$$A_{m+2,n} = \frac{m(m+2) - \nu^2 - n^2}{(m+2)^2 - n^2} A_{m,n} \tag{29}$$

Note that the present solution for $R_n(r)$ starts from $m = 0$ as shown in Eq. (9) while Lamb's solution starts from $m = n$. Lamb's solution can be modified to start from $m = 0$:

$$R_n(r) = \sum_{m=0}^{\infty} A_{m+n,n} \left(\frac{r}{a}\right)^{m+n} \tag{30}$$

Putting $m+n$ in place of m in Eq. (29), we obtain

$$A_{m+n+2,n} = \frac{(m+n)(m+n+2) - \nu^2 - n^2}{(m+2)(m+2n+2)} A_{m+n,n} \tag{31}$$

A comparison of Eqs. (15) and (31) shows that the present solution is identical to Lamb's if the first two coefficients of each solution are given as $A_{n,n} = a^n$, $A_{1+n,n} = 0$, $\alpha_{0,n} = 1$, and $\alpha_{1,n} = 0$. Hence, for the case of $a = b$, in the pit region the present solution is identical to Lamb's and represents the seiching modes in a hemisphere basin. In general, however, the present solution concerns the wave propagation over a pit in an unbounded domain. The present solution can be easily extended to a pit with a different shape by changing the power of r in Eq. (1). In this work, we consider a pit with a parabolic shape with the second power of r. As another example, for a cone-shaped pit, we would use the first power of r.

3.2. Comparison with numerical solutions

For comparison, the analytic solution was compared with an existing numerical solution based on the hyperbolic mild slope equations developed by Copeland [1]. See Suh et al. [12] for more details of the computational procedure used for hyperbolic mild slope equation models. The constant water depth, h_1, was set to 3.2 m, and the relative water depth to $k_1 h_1 = 0.167$ so that the long wave assumption was satisfied. The dimensionless radius of the pit was $b/L_1 = 0.5$, where L_1 is the wavelength in the constant depth region. We tested three different water depths at the center of the pit, h_0: 6.4, 9.6, and 12.8 m. The first two still satisfy the common criterion for long waves, $kh < \pi/10$,

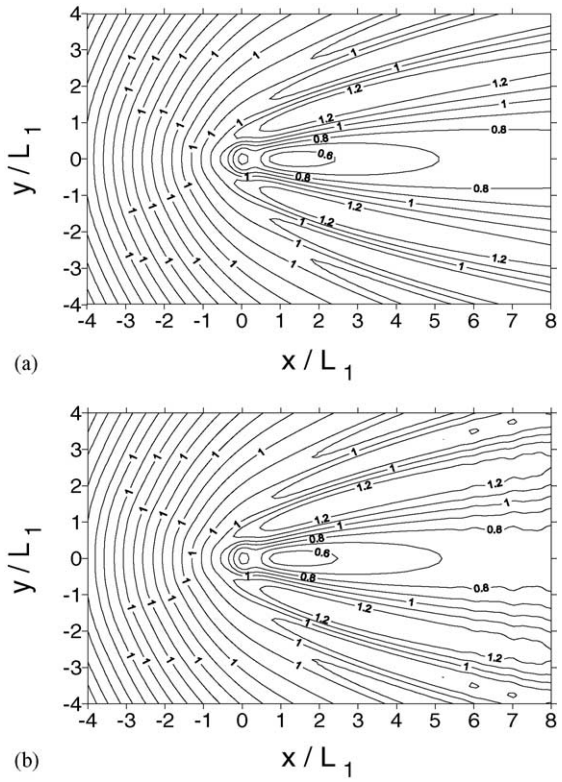

Fig. 2. Contours of diffraction coefficient for a bowl pit with $h_0 = 6.4$ m and $b/L_1 = 0.5$: (a) analytic solution; (b) numerical solution.

while the last one slightly violates the criterion. The results are presented in terms of dimensionless coordinates, x/L_1 and y/L_1.

The analytic solution for η involves an infinite series, but in practice this must be properly truncated. In other words, we must find an integer N that is large enough such that the infinite series in Eqs. (18), (20) and (21) is approximated with the desired accuracy. The number of terms, M, of the truncated Frobenius series of Eq. (9) should also be large enough to give accurate results. Numerical tests for incident waves on constant depth, i.e. Eq. (18), showed that $N = 40$ was enough to give nice sinusoidal waves. In this study, we used $N = 70$ and $M = 30$. The Bessel functions in the analytic solution were computed using the subroutines in [11].

For the numerical solution, the grid spacing was chosen to be $\Delta x = \Delta y = L_1/30$. The time step was chosen for the Courant number $C_r = C_1 \Delta t/\Delta x$ to be 0.2, where C_1 is the wave phase speed in the constant depth region. The incident waves were generated inside the model domain using the technique of Larsen and Dancy [7]. Sponge layers were used at both upwave and downwave boundaries, and reflecting conditions at the side boundaries. The analytic solution was computed from $-4L_1$ to $4L_1$ in the lateral direction. However, the numerical computation was

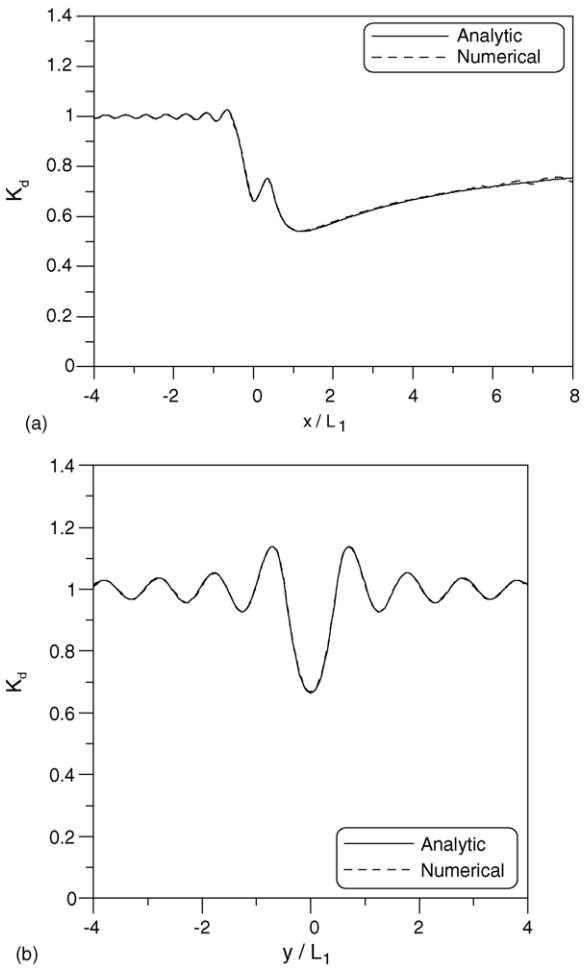

Fig. 3. Comparison between analytic and numerical solutions for diffraction coefficients for a bowl pit with $h_0 = 6.4$ m and $b/L_1 = 0.5$: along (a) x-axis; (b) y-axis.

performed from $-8L_1$ to $8L_1$ and only the results in the range of $-4L_1$ to $4L_1$ were used, in which the effect of the side boundaries was minimal.

Fig. 2 shows a comparison between analytic and numerical solutions in the case of $h_0 = 6.4$ m. The incident wave direction $\theta_0 = 0^\circ$, and the center of the pit is located at the origin. The contour lines indicate the values of the diffraction coefficient, or the wave amplitude relative to the incident amplitude. The agreement between the two solutions is excellent except in the far downwave region, where the numerical solution exhibits some disturbance probably due to small wave reflection from the downwave sponge layer. For more quantitative comparison, the diffraction coefficients were plotted along the x- and y-axis as shown in Fig. 3. The two solutions are almost identical again except in the far downwave region. It can be seen that in front of the pit a partial standing wave system develops, while in the lee of the pit a shadow zone exists in which wave heights are reduced. A small peak of diffraction coefficient appears just in front of the rear end of the pit, i.e. at $x/L_1 \cong 0.4$, probably due to wave reflection from the rear wall of the pit. In the lateral direction, the diffraction coefficient shows a depression at the center of the pit and oscillates with distance from the pit and approaches unity after several wavelengths.

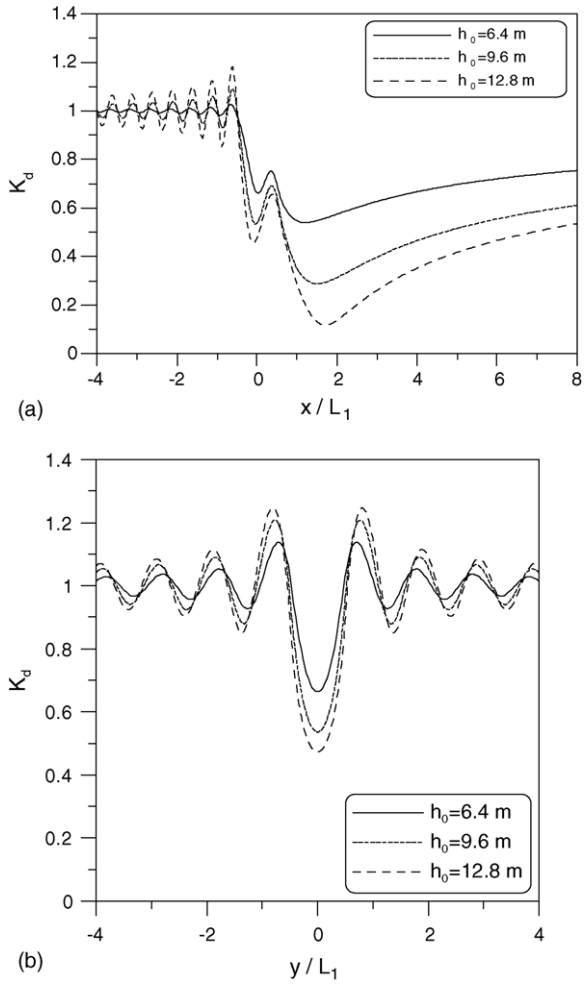

Fig. 4. Comparison of diffraction coefficients among bowl pits with different central depths but with the same radius: along (a) x-axis; (b) y-axis.

Without showing the results, we mention that the results for $h_0 = 9.6$ and 12.8 m also show very good agreement between the analytic and numerical solutions, with only minor differences beginning to appear as the relative water depth in the pit becomes intermediate (i.e. $h_0 = 12.8$ m). These results provide a useful further verification of the accuracy of this numerical implementation for the situation considered. In the following section, we examine the effects of the pit dimensions on the wave scattering using the analytic solution.

3.3. Effects of pit dimensions

Fig. 4 shows diffraction coefficients (i.e. the wave amplitude relative to the incident amplitude) along the x- and y-axis for the cases of $h_0 = 6.4$, 9.6, and 12.8 m with a pit radius of $b/L_1 = 0.5$. As the depth of the pit increases, the partial standing wave (due to reflection) in front of the pit increases, and more wave energy is also scattered laterally due to refraction; thus, there is more of a reduction of wave heights in the shadow zone. The location of the smallest wave height in the shadow zone is shifted backwards as the depth of the pit increases, but the location of the small peak in the pit remains almost constant. The lateral variation of the diffraction coefficient also increases

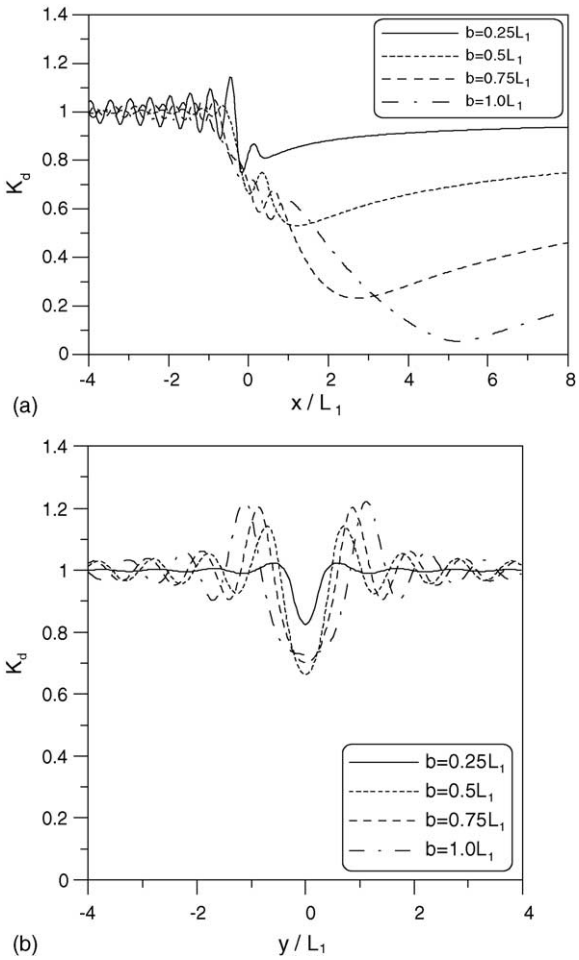

Fig. 5. Comparison of diffraction coefficients among bowl pits with different radii but with the same central depth: along (a) x-axis; (b) y-axis.

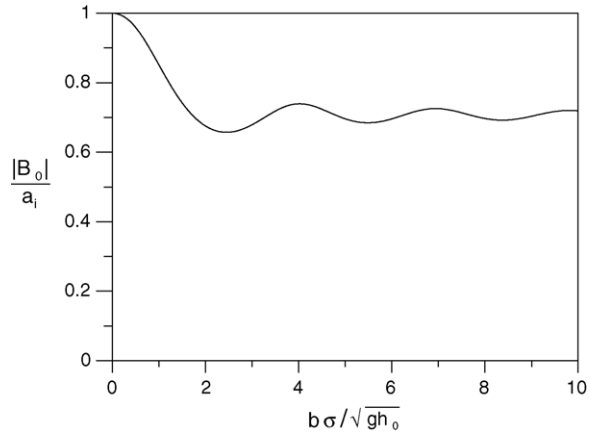

Fig. 6. Dimensionless amplitude of the first wave mode in the region of a pit as a function of dimensionless frequency, $b\sigma/\sqrt{gh_0}$.

with the depth of the pit, showing the locations of its maxima and minima be shifted farther from the pit as the pit depth increases.

Fig. 5 shows diffraction coefficients along the x- and y-axis for the cases of $b/L_1 = 0.25$, 0.5, 0.75, and 1.0 with a pit depth of $h_0 = 6.4$ m. As the pit radius increases with respect to the maximum depth, the slopes within the pit decrease, hence, less wave reflection occurs. Nonetheless, the increased refractive scattering of the larger pits is a greater effect; thus, for larger pits there is still a greater reduction of wave heights in the shadow zone. The location of the smallest wave height in the shadow zone is shifted backwards as the radius of the pit increases. The location of the small peak in the pit is also shifted backwards as the pit radius increases, as expected. As with the pit depth, the lateral variation increases with the radius of the pit. Again as expected, the locations of maxima and minima of the diffraction coefficient are shifted farther from the pit as the radius increases.

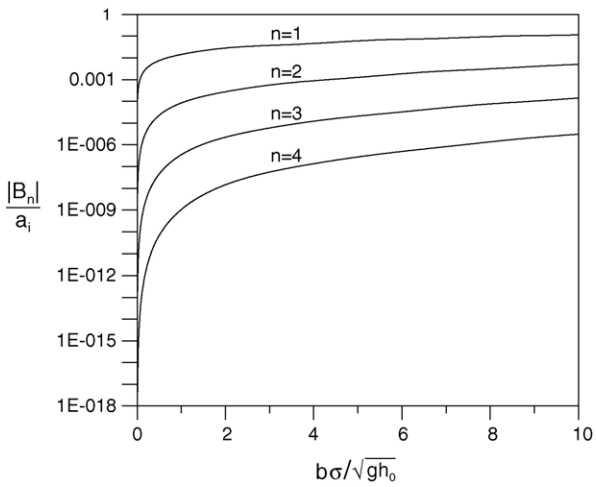

Fig. 7. Dimensionless amplitudes of several higher wave modes in the region of a pit as a function of dimensionless frequency, $b\sigma/\sqrt{gh_0}$.

3.4. Wave attenuation inside pits

When long waves propagate over a submerged island, waves are trapped in the region over the island so that the amplitude of each wave mode is amplified at the resonant frequencies (see Longuet-Higgins [9] and Liu [8]). In the case of a pit, however, we expect wave attenuation in such a way that the wave amplitude becomes smaller than the incident amplitude in the region over the pit. Figs. 6 and 7 show the amplitudes of several wave modes in the region over the pit relative to the incident amplitude as a function of the dimensionless frequency, $b\sigma/\sqrt{gh_0}$. The geometry of the pit is the same as that used to produce Figs. 2 and 3. Calculation was made up to the dimensionless frequency of 10.0 to see the behavior of the amplitudes with the change of the frequency, but the long wave approximation (i.e. $kh \leq \pi/10$) is satisfied only up to the dimensionless frequency of about 2.9 for the largest water depth at the center of the pit.

As shown in Fig. 6, the dimensionless amplitude of the first wave mode ($n = 0$) is unity for very long waves, decreasing to about 0.66 at $b\sigma/\sqrt{gh_0} \cong 2.4$ and bouncing to oscillate around 0.7 for larger frequencies. On the contrary, the amplitudes of the higher modes being very small for very long waves increase monotonically with the frequency as shown in Fig. 7, but they are much smaller than that of the first wave mode. In conclusion, wave attenuation occurs in the region over the pit, as expected.

4. Conclusion

We derived an analytic solution to the mild slope wave equation for long waves propagating over a circular bowl pit located in an otherwise constant depth region. The analytic solution was found to be an extension of Lamb's [6] solution for a hemisphere for specific values of the coefficients in the first two terms of each series solution. The analytic solution was compared with a finite-difference solution of the hyperbolic mild slope equations, and the two solutions were shown to be nearly identical. Hence, the present solution represents a rigorous test case for numerical implementations of the mild slope equation. The effects of the pit dimensions such as the central depth and radius of the pit were also examined, and the variation in wave scattering for different pit configurations was described. Finally, it was found that wave attenuation occurs in the region of the pit in contrast to the wave amplification in the region of a submerged island.

Acknowledgments

KDS thanks God for comforting him with Psalms 40:2 while he was struggling with the pit problem. KDS and THJ were supported by the Brain Korea 21 Project and Korea Ocean Research and Development Institute.

References

[1] G.J.M. Copeland, A practical alternative to the mild-slope wave equation, Coastal Eng. 9 (1985) 125–149.
[2] K. Fujima, D. Yuliadi, C. Goto, K. Hayashi, T. Shigemura, Characteristics of long waves trapped by conical island, Coastal Eng. Jpn. 38 (1995) 111–132.
[3] F.B. Hildebrand, Advanced Calculus for Applications, second ed., Prentice-Hall, Englewood Cliff, New Jersey, 1976.
[4] S. Homma, On the behavior of seismic sea waves around circular island, Geophys. Mag. XXI (1950) 199–208.
[5] I.G. Jonsson, O. Skovgaard, O. Brink-Kjaer, Diffraction and refraction calculations for waves incident on an island, J. Marine Res. 34 (1976) 469–496.
[6] H. Lamb, Hydrodynamics, sixth ed., Dover, New York, 1945.
[7] J. Larsen, H. Dancy, Open boundaries in short wave simulations-a new approach, Coastal Eng. 7 (1983) 285–297.
[8] P.L.-F. Liu, Effects of depth discontinuity on harbor oscillations, Coastal Eng. 10 (1986) 395–404.

[9] M.S. Longuet-Higgins, On the trapping of wave energy round islands, J. Fluid Mech. 29 (1967) 781–821.
[10] D.R. Michalsen, M.C. Haller, K.D. Suh, Erosional hot spot modeling: the impact of offshore borrow pits, J. Coastal Res. Special issue, in press.
[11] W.H. Press, S.A. Teukolsky, W.T. Vetterling, B.P. Flannery, Numerical Recipes in FORTRAN: The Art of Scientific Computing, Cambridge University Press, Cambridge, 1992.
[12] K.D. Suh, C. Lee, Y.-H. Park, T.H. Lee, Experimental verification of horizontal two-dimensional modified mild-slope equation model, Coastal Eng. 44 (2001) 1–12.
[13] A.C. Vastano, R.O. Reid, Tsunami response for islands: verification of a numerical procedure, J. Marine Res. 25 (1967) 129–139.
[14] X. Yu, B. Zhang, An extended analytic solution for combined refraction and diffraction of long waves over circular shoals, Ocean Eng. 30 (2003) 1253–1267.
[15] Y. Zhang, S. Zhu, New solutions for the propagation of long water waves over variable depth, J. Fluid Mech. 278 (1994) 391–406.
[16] S. Zhu, Y. Zhang, Scattering of long waves around a circular island mounted on a conical shoal, Wave Motion 23 (1996) 353–362.